ELSEVIER

Sensors and Actuators B 78 (2001) 144–150

SENSORS AND ACTUATORS B CHEMICAL

www.elsevier.com/locate/sensorb

Influence of gaseous species transport on the response of solid state gas sensors within enclosures

A.M. Lezzi[a,*], G.P. Beretta[a], E. Comini[b], G. Faglia[b,1], G. Galli[a], G. Sberveglieri[b]

[a]*Mechanical Engineering Department, INFM, University of Brescia, Via Branze 38, 25123 Brescia, Italy*
[b]*Chemistry and Physics for Materials Department, INFM, University of Brescia, Via Valotti 9, 25133 Brescia, Italy*

Abstract

The filling of a measurement chamber for gas sensor characterization, with CO diluted in air by the flow-through method is simulated by using a general-purpose CFD code. Numerical data allow to follow the time evolution of CO concentration at any point inside the chamber, thus representing an helpful tool for designing effective test chambers and for interpreting experimental electrical data. In particular, it is shown that CO concentration over the sensor surface increases with time quite slowly, even if the air–CO jet impinges on the device from a short distance. In addition, a comparison of numerical results with experimental data is presented and discussed. © 2001 Elsevier Science B.V. All rights reserved.

Keywords: Gas sensors; Measurement chamber; Mass transfer; Forced convection

1. Introduction

Many contributions can be find in literature devoted to the characterization of gas sensors, but insofar little attention has been paid to space distribution of the examined gaseous species inside measurement chambers and to its evolution in time. In gas sensor characterization by the flow-through method, a mixture of air and the gas to be detected is injected since time t_0 in the test chamber. Denoting the gas concentration in the injected stream as c_0, the average gas concentration in the chamber will tend to c_0 only in a finite lapse of time. Besides, in this time interval, gas concentration inside the chamber may not be uniform. Just as smoke produced by a cigarette which is lighted in a still room: smoke is highly concentrated in the buoyant plume arising from the burning tip, but it has vanishingly small concentration in most of the room. Since the response of solid state gas sensors depends on local gas concentration in a neighborhood of the sensor surface, rather than on the average value in the chamber, it is expected that data collected during characterization be affected by sensor position and concentration transient.

Going back to the smoke plume example, it is apparent as concentration fields are governed by fluid motions: the height the smoke plume rises before becoming unstable and mixing with air depends on the presence and intensity of air currents in the room. Higher air velocities induce a more rapid and efficient mixing. Therefore, analysis of transport phenomena in measurement chambers may represent a valuable tool to assess the influence of geometrical parameters as chamber volume and shape or sensor position, on the dynamic response of the device and to design effective test chambers.

To illustrate this idea, let us consider the following examples. In order to avoid effects due to non uniform gas concentration, it appears reasonable to place the sensor in the air–gas stream, very close to the point of injection and to assume a concentration value equal to c_0 on its surface. Similarly, the concentration transient may be reduced to a value substantially smaller than the sensor response time upon reducing the chamber volume and increasing the volume flow rate through the chamber. That is based on the hypothesis that the concentration transient is not much longer than the ratio between chamber volume and volume flow rate. The soundness of these assumptions can be verified by numerical simulations performed with general-purpose computational fluid dynamics (CFD) codes, which allow to follow the time evolution of species concentration, as well as mixture velocity and temperature in any point inside the chamber.

* Corresponding author.
E-mail addresses: lezzi@bsing.ing.unibs.it (A.M. Lezzi), gfaglia@tflab.ing.unibs.it (G. Faglia).
[1] http://tflab.ing.unibs.it.

PII: S0925-4005(01)00805-X

To substantiate these statements a computational and experimental study of the transient filling of cylindrical test chambers by traces of carbon monoxide diluted in air has been undertaken and its results are reported here. Since computations required several hundreds of hours, the simulations performed insofar are limited in number and based on a simplified model of the characterization process. As a consequence this paper has to be considered as a first contribution to discussion on this subject and a stimulus for further research both numerical and experimental.

Section 2 contains a brief description of the experimental calibration procedure which has been considered for numerical modeling. Section 3 describes the simplified numerical model of the experimental configuration and the approach used to solve it. Finally, in Section 4 the results of numerical simulations are presented and discussed, together with a qualitative comparison with experimental data. As already mentioned at the beginning of this introduction, authors are not aware of contributions in the recent literature on both heat and mass transfer and gas sensing, dealing with unsteady diffusion of a gas carried by a laminar air stream that passes through an enclosure. For this reason in the bibliography, it is listed only a general reference [1] containing a detailed physical and mathematical description of the phenomena addressed by this paper.

2. Experimental

Tin oxide thin films have been deposited through the RGTO technique over alumina substrates 3 mm × 3 mm ×0.25 mm [2]. A Pt thin film was deposited on the back of the substrate as a heater and temperature sensor. The devices were mounted on TO-8 electronic cases and placed inside test chambers. During operation the device local temperature is kept at $T = 400^{\circ}C$, whereas the test chamber is placed inside a thermostatic chamber that keeps the temperature constant at $T = 20^{\circ}C$. Change of electrical resistivity of the device is detected by a volt-amperometric technique at constant voltage. A picoamperometer measures the current that flows across the sensor. More details on the experimental setup can be found elsewhere [3].

During sensor characterization constant flow of synthetic air is maintained across the chamber according to the flow-through method. Traces of CO from certified bottles are introduced in the flow; CO concentration is varied in the range 100–300 ppm. When CO is introduced the sensor conductance increases and, after a few minutes, reaches steady-state conditions. The response time to a given concentration is defined as the time needed to the current to reach 90% of the rising step.

Each CO step lasts 30 min in order for the sensor to reach steady-state conditions. Between each step, dry air flow is restored for 60 min to allow the sensor recovery to initial conditions.

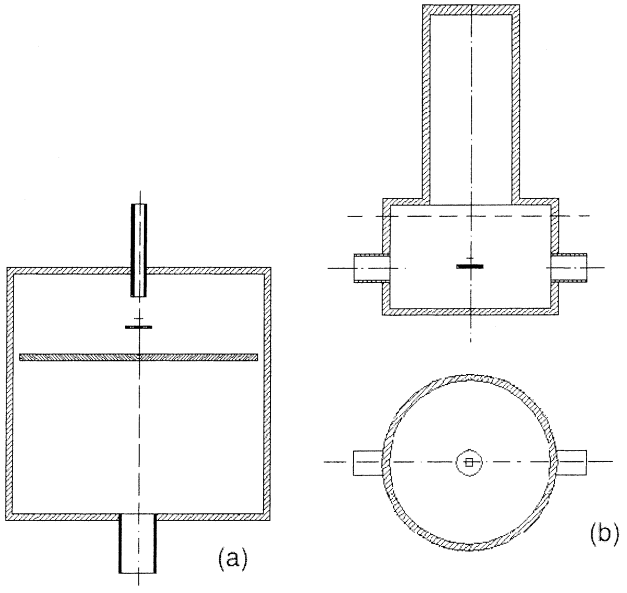

Fig. 1. Measurement chamber models used in simulations. (a) Axisymmetric chamber: air enters from the upper tube and impinges vertically on the sensor surface; (b) chamber with inlet and outlet ports on sidewall. In both configurations, the sensor case is represented as a small disk. The sensor is represented either as a thin disk or a thin square plate in configurations (a) and (b), respectively.

Measurements have been made using two different test chambers. Most of data have been collected with a cylindrical test chamber 1000 cm^3 in volume, which is sketched in Fig. 1(a). The sensor case is mounted on a plate which is placed at about two-third of the chamber height. Inside the chamber, a 4 mm i.d. stainless steel tube is connected to the chamber inlet port. The tube outlet is placed 10 mm away from the sensor and tilted from parallel to perpendicular to the sensor surface. In the tests performed, beside the relative inclination of the impinging flow, the total flow has been varied in the range 100–500 sccm.

Some measurements have been carried out in the chamber shown in Fig. 1(b). The chamber, which is made by two superposed cylinders of different diameter, has a total inner volume equal to 233 cm^3 approximately. The axes of the 10 mm i.d. inlet and outlet tubes coincide. The sensor is placed on the chamber vertical axis, a few millimeters above the inlet port axis, and the incoming air stream flows parallel to its surface.

3. Numerical model

Numerical simulations were performed using Fluent/UNS v. 4.2, a general-purpose CFD package with capabilities of modeling a large variety of physical phenomena — including heat and mass transfer both in laminar and turbulent flows — in complex geometries. Fluent/UNS solves mass, momentum, energy and chemical species transport equations on unstructured grids using a finite volume discretization technique.

Since a detailed simulation of the filling of a test chamber may require hundreds of hours of computing time, in this preliminary work geometrical and physical simplifications have been introduced in order to reduce the computational effort. Thus, the fluid flowing through the chamber is modeled as a dilute binary mixture of CO in dry air, with constant diffusion coefficient $D = 2.88 \times 10^{-4}\ \mathrm{m^2\ s^{-1}}$. Although the sensor is operated at 400°C, inducing in this way significant changes of gas density in its surroundings, in all computations a uniform temperature equal to 20°C is assumed. This avoids solution of the energy equation and use of the ideal gas law to keep track of density changes. As a matter of fact, under these conditions the flow can be considered as nearly incompressible and the mixture density can be set constant. That reduces both the number and the complexity of the equations to be solved.

All but one simulations performed in the numerical study are restricted to an axisymmetric configuration in order to reduce computing time by solving a 2D problem instead of a fully 3D one. In Fig. 1(a), a sketch of the simplified model of the measurement chamber used in numerical simulations is shown. To preserve the axial symmetry of the cylindrical chamber, both the sensor and the case are represented as two horizontal disks placed on the chamber axis. The incoming air–CO jet impinges vertically on them and the jet and the chamber axes coincide. No other directions of incidence are considered. The computational domain consists of the space bounded by the chamber top and lateral wall and by the plate. The volume of this region is 333 $\mathrm{cm^3}$. A 40 mm long section of the inlet-tube is included in the computational domain — 30 mm of this section extend outside the chamber. The outflow is through the 3 mm gap between the plate and the sidewall of the chamber. A preliminary test showed that neglecting to consider the space below the plate has practically no effects on numerical results.

Boundary conditions are the following: at the tube inlet section uniform velocity and CO concentration are imposed; uniform ambient pressure is imposed at the outflow. All computations are performed on an unstructured, hybrid grid. A large number of cells is placed around the sensor and between the sensor and the inlet-tube outlet where the largest velocity and CO concentration gradients occur. Triangular and rectangular cells are used inside the chamber and the inlet-tube, respectively. The grid size is about 10^4 cells which allows a good trade-off between accuracy and computing time. Calculations were performed on a PC equipped with an Intel Pentium 233 processor and 128 MB of RAM and required about 400 h.

In addition to 2D simulations, a single 3D simulation was carried out for the test chamber shown in Fig. 1(b). This configuration is not axisymmetric because of the inlet and outlet ports on the chamber sidewall. However, the vertical plane containing the cylinders axis and the ports axis is a plane of symmetry. Taking advantage of this fact, the computational domain is restricted to only half of the chamber. An unstructured grid made of tetrahedral cells is used. Cell density is higher in the region occupied by the stream between the inlet and outlet tubes, particularly nearby the device, whereas quite large cells are used inside the upper cylinder where the fluid hardly moves. The grid size is 27×10^4 and requires a machine with a large RAM. For this reason, the 3D simulation was performed on a Silicon Graphics Indigo 2 workstation equipped with 384 MB of RAM and took about 670 h of computing time to follow 425 s of real time.

4. Results and discussion

4.1. Numerical results

For the axisymmetric configuration numerical results have been obtained for five flow rates ranging from 100 to 500 sccm. In all cases, flow regime is laminar, the jet Reynolds number ranging between 36 and 180. For each flow rate simulation is a two-step process: at first, steady-state velocity and pressure fields for pure dry air inflow are computed to reproduce the conditions in the test chamber at the end of the cleaning phase. Then these fields are used as initial condition to determine time evolution of CO concentration field. An additional set of simulations have been performed by removing the chamber upper wall and sidewall, but retaining the plate (unconfined case).

With reference to Figs. 2–4, the flow field inside the test chamber can be described as follows. On the basis of fluid motions, three distinct zones can be identified. The first one is the gaseous jet that exits from the inlet-tube and,

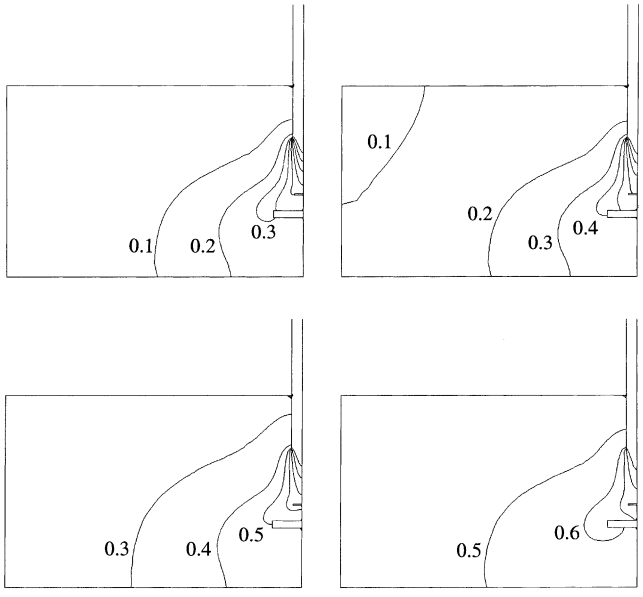

Fig. 2. Contours of constant CO concentration inside test chamber for 100 sccm flow rate. Increments are uniform and equal to $c_0/10$, where c_0 is the CO concentration at the inlet port. From left to right and from top to bottom, $t = 10$, 30, 60, and 120 s. Time is measured from the instant the air–CO mixture enters the inlet-tube.

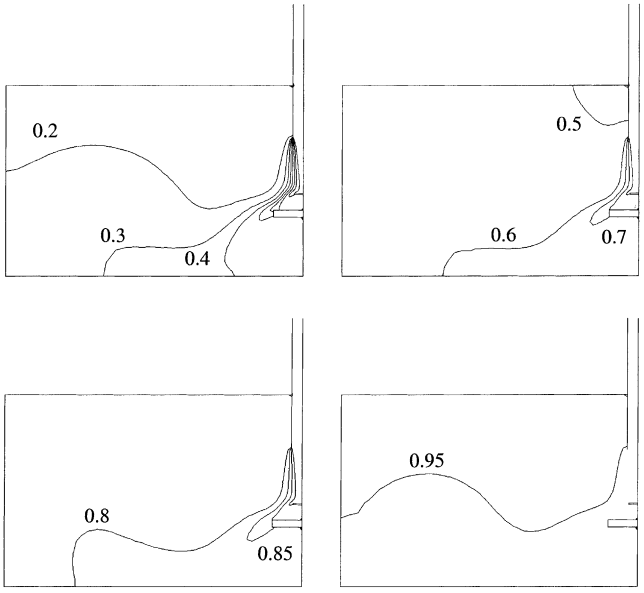

Fig. 3. As Fig. 2 for 500 sccm flow rate. Increments are equal to $c_0/10$ for $t = 10$ and 30 s, and equal to $c_0/20$ for $t = 60$ and 120 s.

approaching the sensor surface, decelerates and spreads radially towards the outlet gap (see the blackened area in Fig. 4). In addition to the jet, there are two regions of fluid characterized by a slowly circulating motion: one is underneath the sensor case, while the other occupies most of the chamber upper part. There is no mixing of fluid among the three regions: any macroscopic fluid particle, or element, that enters the chamber leaves it through the peripheral gap. At the end of the cleaning phase, as soon as the air–CO mixture is injected into the chamber at constant concentration c_0, CO is advected by the flow field and in short time it occupies the whole jet region. Local concentration of CO inside this region depends on jet flow rate and spreading. In any case, it is always less than c_0.

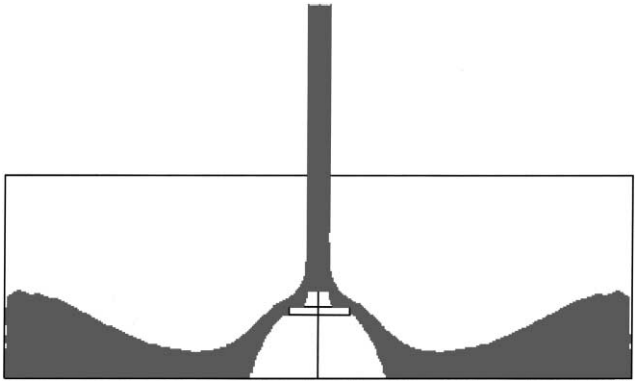

Fig. 4. Sketch of the jet: steady-state solution for pure dry air inflow and 100 sccm flow rate. The blackened area represents approximately the region occupied by the fluid passing through the chamber. Two other regions are observed: the mid and upper part of the chamber and the zone underneath the sensor case. In these two regions, the fluid is in slowly circulating motion.

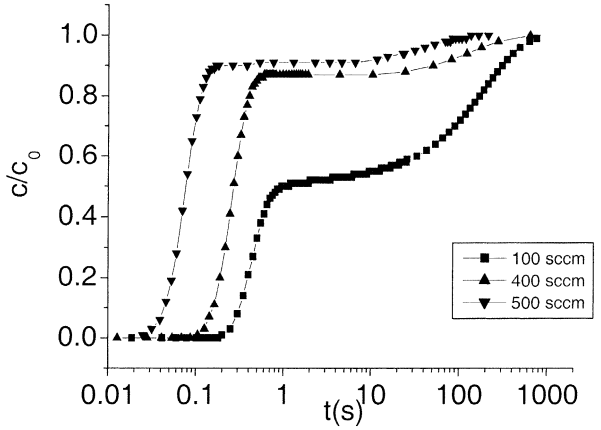

Fig. 5. Time history of normalized surface average of CO concentration on the sensor upper surface for jet flow rate equal to 100, 400 and 500 sccm.

In Figs. 5 and 6, it is shown the numerically calculated time history of average CO concentration on the sensor upper surface, normalized with respect to inlet concentration c_0. It is evident that the growth of CO concentration at the sensor surface is a two-step process. The first steep increment in the curves corresponds to the advection of CO from the inlet-tube towards the sensor and, successively, towards the outlet. In a time interval of the order of 0.1–1 s, CO concentration at the sensor surface reaches a sort of "saturation value" c_u — plateaus in Figs. 5 and 6 — which is an increasing function of jet flow rate. If the sensor and the jet were not confined within an enclosure the "saturation" value c_u would be the CO concentration at the sensor surface at steady-state. This conclusion has been verified by performing a few simulations where the upper and the lateral walls of the chamber were not introduced.

As an example, results for 100 sccm flow rate are shown in Fig. 6, where time history of CO concentration on the sensor surface for the confined and unconfined cases are compared. At the beginning the two curves coincide and

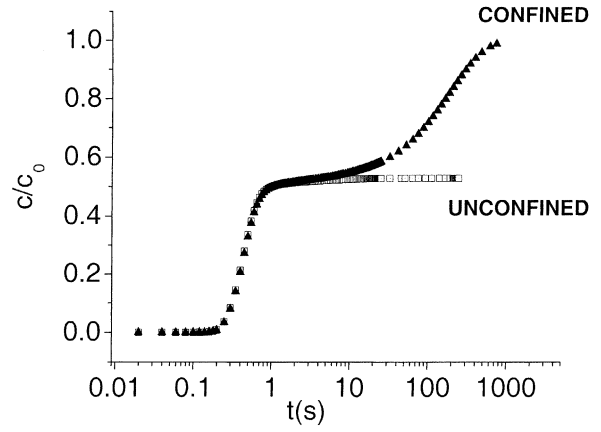

Fig. 6. Time history of normalized surface average of CO concentration on the sensor upper surface for 100 sccm flow rate. Solid triangle: standard conditions; open square: test chamber without cover and sidewall.

represent the transient filling of the jet region with CO. In the unconfined case, a steady value (c_u) is attained in a short time. In the confined case, CO concentration curve flattens out around c_u at first, then keeps on growing, although at a much slower pace.

The second increment, which is apparent in Figs. 5 and 6, corresponds to the process of filling of the entire chamber with CO. This process is much slower than the first one, being characterized by a time scale of a few minutes. It can be explained as follows. If species diffusion were absent, CO would be found only inside the jet (i.e. blackened region in Fig. 4) and no CO would ever enter the two regions of recirculation. However, since molecular diffusion does take place, CO diffuses from the jet into those regions where it accumulates until it reaches concentration c_0 everywhere. The circulatory fluid motion in the zones external to the jet plays an important role in the process. Firstly, it redistributes CO diffused across the jet boundary, over the entire region of recirculation. Secondly, the removal of CO from the jet boundaries maintains the concentration gradients across the jet boundaries high, thus enhancing diffusion fluxes. Motion in the recirculation regions is induced by the jet: the higher the jet flow rate, the stronger are the circulatory motions. That yields in turn a shorter filling time, as it is easily observed in Fig. 5.

As mentioned in Section 3, due to the extremely long computing time required by the fully 3D configuration, only one simulation has been carried out for the test chamber of Fig. 1(b). The case considered is for a jet flow rate equal to 300 sccm. The flow regime is laminar, since the jet Reynolds number is approximately equal to 53.

In this case also, the velocity and pressure fields at the end of the cleaning phase (pure dry air inflow) are determined by running the steady solver of the Fluent package. Then they are used as initial condition for the unsteady computation, during which air–CO mixture is injected into the chamber.

The time evolution of CO concentration field in the chamber and on the sensor surface, in particular, can be described along the same lines as for the axisymmetric case. However, it is worthwhile to underline some quantitative differences that point out the importance of chamber shape and sensor position.

In this configuration, the inlet jet does not impinges normally on the sensor, but flows almost parallel to its surface. In addition, the sensor surface is not placed on the jet axis, but displaced towards its boundary. Looking at velocity distribution inside the chamber it is apparent that the jet tends to flow underneath the sensor case, close to the chamber bottom. As a result CO concentration is higher below the case than above it, where the sensor is located (see Fig. 7). Therefore, it can be concluded that in this chamber the sensor surface is placed in a peripheral position with respect to the air–CO inlet stream.

The effect of sensor position on the time history of average CO concentration on its surface can be appreciated in Fig. 8. It is recognizable the initial rapid increment

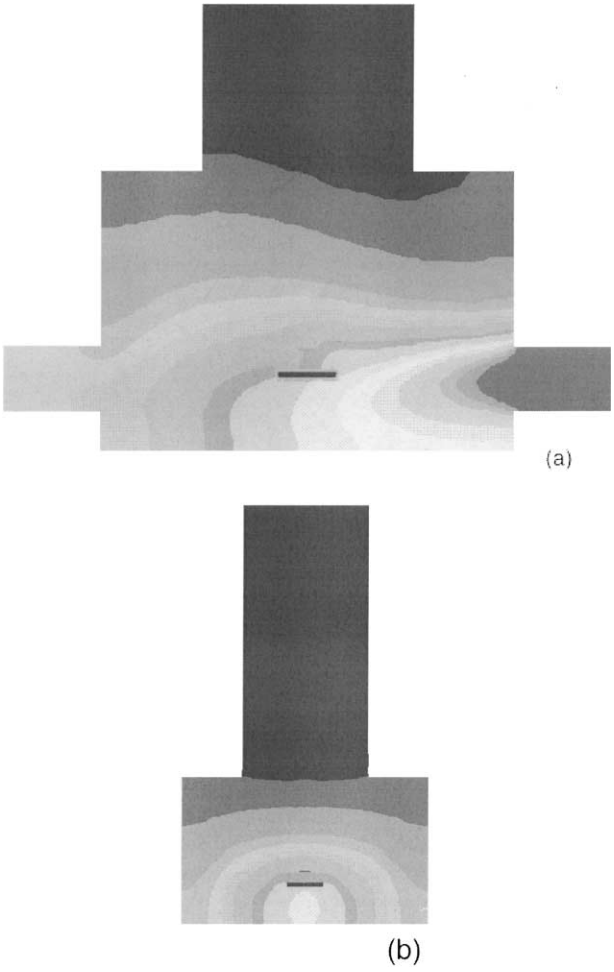

Fig. 7. Contours of constant CO concentration inside test chamber of Fig. 1(b) at 7.5 s, since the instant the air–CO mixture enters the inlet-tube. Jet flow rate equal to 300 sccm. Increments are uniform and equal to $c_0/20$, where c_0 is the CO concentration at the inlet port: (a) vertical plane containing the inlet and outlet tubes axis; (b) vertical plane perpendicular to the inlet and outlet tubes axis.

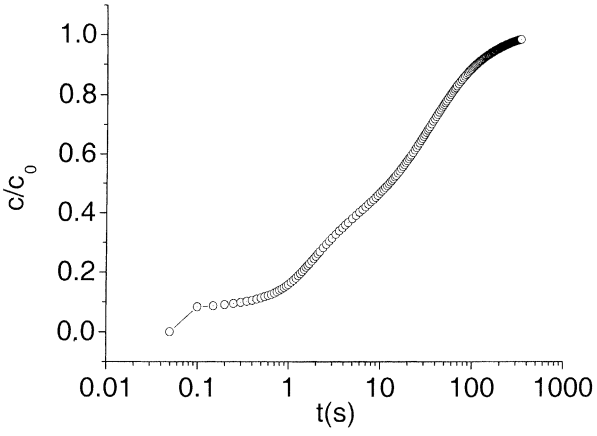

Fig. 8. Test chamber of Fig. 1(b). Time history of normalized surface average of CO concentration on the sensor upper surface for jet flow rate equal to 300 sccm.

towards the first "saturation" value c_u, however, in this case c_u is only 10% of the inlet concentration c_0.

A final remark can be made about the time required to reach a uniform CO concentration equal to c_0 everywhere in the chamber. Numerical results for the same inlet flow rate indicate a "filling" time of about 4 min for test chamber in Fig. 1(a) and of about 6 min for test chamber in Fig. 1(b) which, however, is smaller in volume — 70% of the volume of the axisymmetric chamber. This puzzling result can be explained upon taking into account both the shape of chambers and the velocity field inside them. Inside the upper cylinder in Fig. 1(b), fluid is at rest for all practical purposes: there is no fluid circulation to enhance redistribution of CO diffused from the lower cylinder. As a consequence, the filling of the upper part depends only on molecular diffusion which is a much slower process than advection. This results suggests to avoid measurement chambers where zones of stagnant fluid may form: the flow field inside the chamber has to favorite as much as possible fluid circulation and mixing.

4.2. Experimental results

The detection mechanism of the sensor is based on gas/surface reactions that modulate the height of the energy barrier seen by charged carriers at the interface between grains. When CO is introduced the barrier reduces, since CO consumes ionosorbed oxygen ions producing CO_2. The reaction route and kinetic are a limiting factor in the energy barrier dynamic behavior. Furthermore the conductance G is an exponential function of the energy barrier qV_S

$$G \propto e^{-qVs/kT}$$

Therefore, a direct connection between the instantaneous CO concentration in the sensor surroundings and the sensor conductance can be hardly made. Nevertheless it is interesting to compare sensor electrical output as recorded in experimental tests with CO concentration on the sensor surface as predicted by numerical simulations.

The experimental data plotted in Fig. 9 represent the time history of the normalized sensor response $(I - I_0)/(I_{max} - I_0)$, where I is the current flowing through the tin oxide film when CO is injected in the chamber, I_{max} the maximum sensor response and I_0 the sensor response at pure dry air inflow. Data were collected in a measurement chamber similar to the one in Fig. 1(a) for 100, 200, 300, 400 and 500 sccm jet flow rates. Upon comparing Figs. 5 and 9, it is apparent that the normalized sensor response grows much more slowly than the normalized CO concentration on the sensor. The growth is more rapid for higher flow rates, which is in agreement with numerical predictions. It seems that both the sampling rate and the sensor response time are not sufficiently rapid to follow the first steep increment of CO concentration on the sensor. Therefore, for all practical purposes, the air–CO mixture injection can be considered as a process that changes instantaneously CO concentration near the sensor from zero to a finite value c_u, smaller than

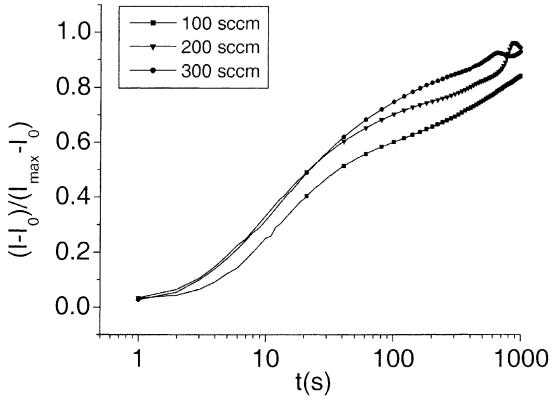

Fig. 9. Axisymmetric chamber. Experimental time history of normalized sensor response for jet flow rate equal to 100, 200 and 300 sccm.

inflow concentration c_0; the first points of the experimental curves represent the device response to a step function whose value is unknown. At later times, instead, the increment of the electrical output is also a result of the slowly growth of CO concentration towards the limit value c_0.

The last observation is confirmed by a series of experiments that have been carried out with the test chamber cover removed. In this configuration, the measurements are affected by a greater noise which is due to changes in the environment around the open chamber (during the tests, the thermostatic chamber also was kept open for safety reason). In Fig. 10, the sensor response $I - I_0$, normalized with respect to I_0, is plotted for closed and open chamber (confined and unconfined case, respectively). Inlet flow rate is 300 sccm. As discussed above, in the unconfined case CO concentration on the sensor never reaches the inlet value c_0, whereas in a closed chamber this value is eventually attained. Thus, the device response is expected to be smaller for the uncovered chamber than for the covered one. As shown in Fig. 10, this is what has been found experimentally. In Fig. 11, it is shown a quantitative comparison between numerical predictions and experimental data. Open symbols

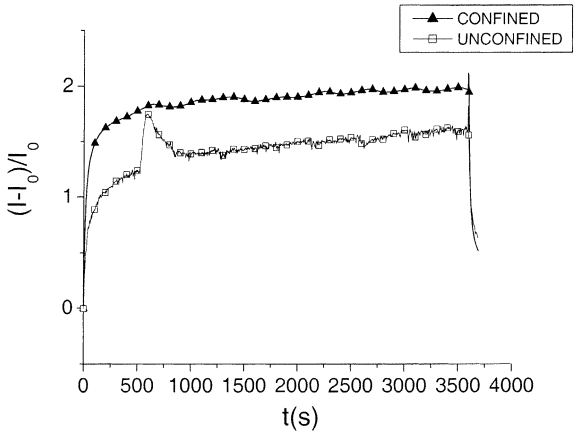

Fig. 10. Axisymmetric chamber. Comparison between time history of normalized sensor response as collected in a closed chamber and in chamber with the cover removed. Jet flow rate equal to 200 sccm.

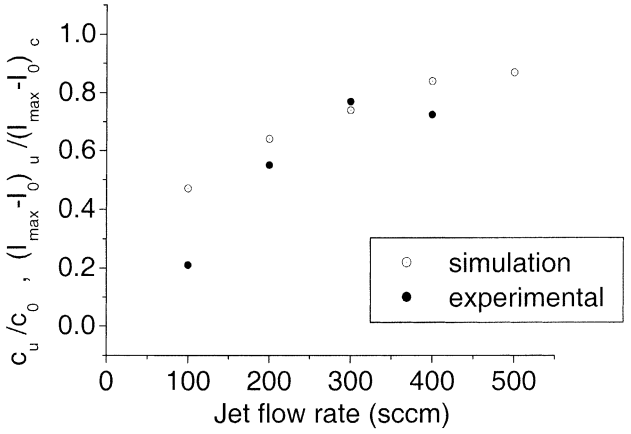

Fig. 11. Axisymmetric chamber. Comparison between experimental data and numerical results. Solid circle: ratio between the maximum device responses measured with the test chamber uncovered and covered, respectively. Open circle: ratio between asymptotic values of surface average of CO concentration on the sensor calculated for the unconfined and the confined configurations.

represent the ratio between c_u and c_0, i.e. the asymptotic values of average CO concentration on the sensor surface for the unconfined and confined case, respectively — for different jet flow rates, as computed in simulations. Solid symbols, instead, represent the ratio between the maximum device response $I_{max} - I_0$ for the uncovered and covered chamber, respectively, as determined in experiments. With the exception of the datum for 100 sccm flow rate, the agreement can be considered satisfactory.

With regard to the fully 3D test chamber, comparison of numerical results with experimental data is unsatisfactory: the sensor electrical response grows in time faster than numerically predicted CO concentration. In particular, the electrical output attains a steady value about 2 min before CO concentration on the sensor surface reaches the injection value c_0. Differences are believed to be due to mixed convection effects which are not accounted for in the numerical model. As a matter of fact, a buoyant plume is expected to rise from the hot sensor, which is maintained at 400°C. The plume should induce a circulating motion inside the upper cylinder, thus enhancing CO redistribution within the chamber and reducing the time of complete filling with CO.

5. Conclusions

Gas sensor characterization in a measurement chamber by the flow-through method has been numerically simulated with a two-fold goal. On one hand we wanted to verify the extent to which results yielded by CFD analysis may be useful in interpreting experimental results. On the other hand, we aimed at obtaining the time history of average gas concentration on the sensor surface as determined by fluid motions inside the chamber, sensor position, chamber volume, etc. and to compare it with the device electrical response.

Numerical results suggest the important role that geometrical parameters such as the measurement chamber volume, the chamber shape and the inlet and outlet position play on the development of the fluid flow and the gas concentration fields inside the chamber. In particular, it has been shown that even in the most favorable configuration, i.e. air–CO stream impinging vertically on the sensor surface from a short distance, CO concentration on the sensor surface reaches almost immediately a value c_u which is smaller than the concentration at the inlet c_0. The concentration of injection is attained rather slowly, in a time interval that appears comparable with the sensor response time. The value c_u is an increasing function of flow rate through the chamber, whereas the concentration transient is a decreasing one. For poorly designed test chambers, characterized by large volumes of almost stagnant fluid and/or by a peripheral position of the sensor with respect to the air–CO stream, CO concentration on the sensor surface may keep on increasing for a very long time. In these cases, the device response time — defined as the time needed to the electrical output to reach 90% of steady-state value — is more a measure of CO concentration transient inside the chamber than a characteristic feature of the device.

Experimental results show some evidence of the mechanisms described through the numerical study. We refer, in particular, to the differences in the sensor response between covered and uncovered test chamber configurations. These tests are also characterized by a satisfactory quantitative agreement between experimental data and numerical predictions. In other tests — test chamber with inlet and outlet ports on the lateral wall — the comparison between experiment and simulation yields unsatisfactory results.

As an attempt to explain gas sensor response behavior during characterization by the flow-through method, this paper is certainly incomplete. In the first place, the number and type of simulations is limited. Secondly, buoyancy effects due to the sensor high temperature are not accounted for. In spite of these shortcomings, results obtained insofar shed some light on the mechanisms by which geometrical parameters as the chamber volume and shape, or the sensor position, and flow variables as the jet flow rate can influence the sensor electrical response and are sufficiently interesting to warrant further investigations.

In conclusion, it has been shown that CFD analysis of flow, temperature and species concentration fields in the environment nearby a gas sensor can be an helpful tool to understand and interpret experimental electrical data. Besides, it can suggest to researchers criteria for designing of effective test chambers.

References

[1] R.B. Bird, W.E. Stewart, E.N. Lightfoot, Transport Phenomena, Wiley, New York, 1950.
[2] G. Sberveglieri, Recent developments in semiconducting film gas sensors, Sens. Actuators B 23 (1995) 103–109.
[3] G. Sberveglieri, L. Depero, S. Groppelli, P. Nelli, WO_3 sputtered thin films for NO_x monitoring, Sens. Actuators B 26/27 (1995) 89–92.